ACS APPLIED MATERIALS & INTERFACES

Research Article

www.acsami.org

One-Step Preparation of Silver Hexagonal Microsheets as Electrically Conductive Adhesive Fillers for Printed Electronics

Hu-Ming Ren,[†,‡] Ying Guo,[†,‡] Sheng-Yun Huang,[†,‡] Kai Zhang,[§] Matthew M.F. Yuen,[§] Xian-Zhu Fu,*[,†,‡] Shuhui Yu,*[,†,‡] Rong Sun,*[,†,‡] and Ching-Ping Wong[∥,⊥]

[†]Shenzhen Institutes of Advanced Technology, Chinese Academy of Sciences, Shenzhen 518055, China

[‡]Shenzhen High Density Electronic Packaging and Device Assembly Key Laboratory, Shenzhen 518055, China

[§]Department of Mechanical and Aerospace Engineering, Hong Kong University of Science and Technology, Hong Kong, China

[∥]Department of Electronics Engineering, The Chinese University of Hong Kong, Hong Kong, China

[⊥]School of Materials Science and Engineering, Georgia Institute of Technology, Atlanta, Georgia 30332, United States

Supporting Information

ABSTRACT: A facile one-step solution-phase chemical reduction method has been developed to synthesize Ag microsheets at room temperature. The morphology of Ag sheets is a regular hexagon more than 1 μm in size and about 200 nm in thickness. The hexagonal Ag microsheets possess a smoother and straighter surface compared with that of the commercial Ag micrometer-sized flakes prepared by ball milling for electrically conductive adhesives (ECAs). The function of the reagents and the formation mechanism of Ag hexagonal microsheets are also investigated. For the polyvinylpyrrolidone (PVP) and citrate facet-selective capping, the Ag atoms freshly reduced by N_2H_4 would orientationally grow alone on the {111} facet of Ag seeds, with the synergistically selective etching of irregular and small Ag particles by H_2O_2, to form Ag hexagonal microsheets. The hexagonal Ag microsheet-filled epoxy adhesives, as electrically conductive materials, can be easily printed on various substrates such as polyethylene terephthalate (PET), epoxy, glass, and flexible papers. The hexagonal Ag microsheet filled ECAs demonstrate lower bulk resistivity (approximately 8×10^{-5} Ω cm) than that of the traditional Ag micrometer-sized-flake-filled ECAs with the same Ag content of 80 wt % (approximately 1.2×10^{-4} Ω cm).

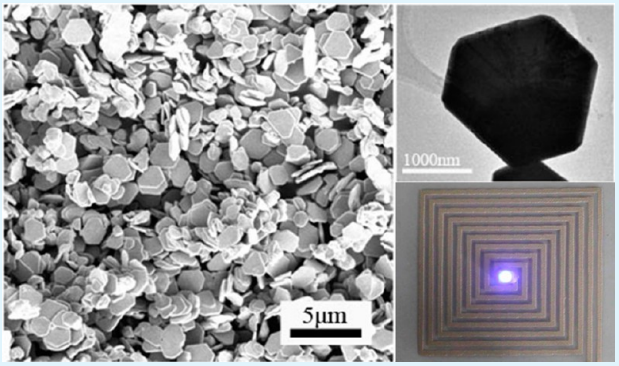

KEYWORDS: *Ag hexagonal flake, nanoplate, facet selective growth, electrically conductive adhesive, printed electronic*

1. INTRODUCTION

Printed electric technologies have received increasing interest due to their unique advantages such as simple fabrication processes, low cost, environmental friendliness,[1−5] and excellent suitability to various substrates including flexible substrates.[6−9] Electrically conductive adhesives (ECAs) and inks (ECIs) are usually used to form high electrically conductive tracks used to connect the electrical parts in the printed devices. ECAs commonly offer sufficiently strong adhesion between the conductive tracks and the substrates that they do not need to be sintered at high temperature like the conventional ECIs.[10,11] ECAs composed of polymer matrix and electrically conductive fillers have been also widely used in the electronics industry.[12−14] The polymer matrix usually consists of polymer resin (epoxy, phenolic, polyurethane, etc.), curing agent, coupling agent, and thinner, which provide mechanical strength and adhesion. The fillers are conductive particles such as metallic particles (gold, silver, copper, etc.), carbon materials (graphene, carbon cubes, carbon fibers, etc.), or conductive metal oxides, which provide electrical conductivity.

Silver is the best choice for ECAs when compared with other electrically conductive fillers because of its high electrical and thermal conductivity, chemical stability, relatively low cost, and the fact that its oxide also shows good conductivity.[15] Micrometer-sized flaky silver fillers are widely used in current commercial ECAs because their face-to-face contact leads to a much larger interface area for current conduction relative to the nanosized fillers. The silver flakes for ECAs are traditionally prepared in two steps including wet chemical reduction to obtain silver powders followed by mechanical ball-milling to form flaky morphology. The contact area of the ball-milled silver flakes could be enhanced compared with that of the precursor silver powders. However, the ball-milled silver flakes' surface is usually still rough and not smooth enough, which easily results in dot-to-dot contact between silver plates.[16] In addition, the ball-milling process easily introduces impurities

Received: April 24, 2015
Accepted: May 29, 2015
Published: May 29, 2015

DOI: 10.1021/acsami.5b03571
ACS Appl. Mater. Interfaces 2015, 7, 13685−13692

such as organic lubricant, which is facially attached to the surface of silver plates and would reduce the conductivity of ECAs.[1] Lots of efforts have been devoted to fabricating silver nanoplates[17−22] such as uniform triangular nanoplates[23−25] and hexagonal nanoplates.[26] Comparing the silver nanoplates, it is still a challenge to prepare uniform and regular silver microsheets in solution, although a few micrometer-sized silver sheets have been successfully fabricated with irregular or mixed regular morphologies in pioneering work in recent years.[27−30]

Herein, we report the one-pot wet chemical synthesis of micrometer-sized and uniform hexagonal silver sheets as ECA fillers for printed electric applications. The preparation method is facile and occurs in aqueous solution at room temperature using silver nitrate ($AgNO_3$), polyvinylpyrrolidone (PVP, K30), sodium citrate, sodium borohydride ($NaBH_4$), hydrogen peroxide (H_2O_2), and hydrazine hydrate (N_2H_4) as the reagents. It is easy to scale up the method to produce silver hexagonal microsheets. The produced micrometer-sized silver flakes are nearly uniform hexagonal sheets with smooth and straight surfaces, the size of more than 1 μm, and the thickness of about 200 nm. The hexagonal silver microsheet filled ECAs could be easily printed on various substrates such as polyethylene terephthalate (PET), epoxy, glass, and flexible paper, and hexagonal silver microsheet filled ECAs demonstrate considerably higher electrical conductivity than that of commercial ball-milled silver-flake-filled ECAs.

2. EXPERIMENTAL SECTION

2.1. Materials. Silver nitrate ($AgNO_3$), polyvinylpyrrolidone (PVP, K30) and hydrazine hydrate ($N_2H_4{\cdot}H_2O$, 85 wt %) were purchased from the Sinopharm Chemical Reagent Company. Sodium borohydride ($NaBH_4$), sodium citrate, hydrogen peroxide (H_2O_2, 30 wt %) were purchased from the Shanghai Lingfeng Company. The epoxy resin (E51), hexahydro-4-methylphthalic anhydride (HMPA), and 1-cyanoethyl-2-ethyl-4-methylimidazole (2E4MZ-CN) were purchased from the Shell Chemical Company. All chemicals were analytical grade and used as received without further treatment.

2.2. Synthesis of Silver Microsheets. A standard process for the fabrication of silver microsheets is presented in the following. A total of 20 mmol of $AgNO_3$ and 1.5 mmol of PVP were mixed in 100 mL of water under vigorous magnetic stirring at room temperature in air. After $AgNO_3$ and PVP were completely dissolved, 4 mL of sodium citrate (0.3M), 0.5 mL of $NaBH_4$ (0.02M), and 10 mL of H_2O_2 were added into the mixed solution. After 0.5 h, 55 mL of $N_2H_4{\cdot}H_2O$ solution was rapidly injected into the above-mentioned mixture at room temperature. The mixed solution then became gray, indicating the formation of metallic silver powders. After 2 h, the reacted solution was centrifuged, and the precipitate was washed with DI water several times. Finally, the product was dried in air at 60 °C for 5 h.

2.3. Preparation of ECAs and Pattern Formation. The polymer matrix was composed of epoxy resin (E51), curing agent (HMPA), and catalyst (2E4MZ-CN) with a ratio of 8:2:0.1. The micrometer-sized silver fillers were then added into the viscous polymer matrix, and the matrix was stirred uniformly. The content of the silver filler was kept at 80 wt % in the total amount of electrically conductive adhesives (ECAs). The conductive patterns that connected the LEDs on different substrates were obtained by screen printing the ECAs on the substrates, mounting the LEDs on the electrodes, and then curing at 150 °C for 2 h.

2.4. Characterization and Measurement. Scanning electron micrographs (SEM) and energy-dispersive spectroscopy (EDS) of the silver microsheets were analyzed by a scanning electron microscope (FEI Nova NanoSEM450) with EMAX250. The selected-area electron diffraction (SAED) pattern and transmission electron microscopy (TEM) images were obtained by a high-resolution transmission electron microscope (FEI Tecnai G2 F20 S-Twin). Atomic force microscopy (AFM) images were observed using an AFM DI Multimode. X-ray diffraction (XRD) patterns were recorded by an X-ray diffractometer (Rigaku D/MAX-2500) operated under Cu radiation; the diffraction angle covered 20−80° with a step size of 0.02°. UV−vis spectra were recorded on an SHIMADZU UV-2550 UV−vis spectrometer. Fourier transform infrared (FT-IR) spectra were recorded between 4000 and 400 cm^{-1} using an FT-IR Bruker Vertex 70. The resistance of the ECAs was measured by a Keithley 2000 multimeter with four-point probes.

3. RESULTS AND DISCUSSION

3.1. Characterization of Silver Microsheets. It is clearly observed in Figure 1a that the as-prepared silver sheets are

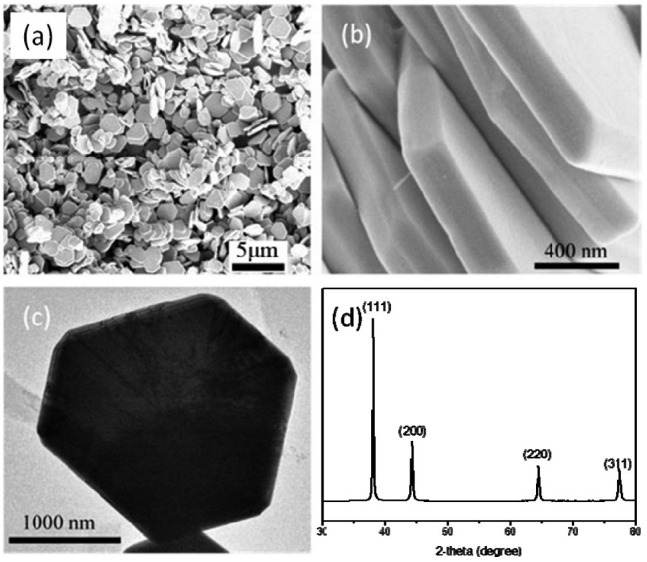

Figure 1. (a,b) SEM and (c) TEM images and (d) the XRD pattern of the as-prepared silver microsheets.

uniform and regularly hexagonal, with a particle size larger than 1 μm. The surface of the Ag microsheets is very smooth and straight. The thickness of the as-prepared Ag sheets is about 200 nm, as shown in Figure 1b. Relative to the previously reported micrometer-sized silver sheets,[27−30] the as-prepared Ag sheets are more uniform and thicker. Figure 1c shows a typical TEM image of an individual as-prepared silver sheet. Similar to the results from the previous report on silver nanosheets,[18,30,31] there are some randomly distributed and continuous lines on the surface that originated from the thin crystal bending. Figure S1 in the Supporting Information displays the corresponding SAED pattern, which is measured by directing the incident electron beam perpendicular to the as-prepared silver sheets. The hexagonal symmetry diffraction spots indicate the face-centered cubic (fcc) crystalline structure of the as-prepared silver sheets.

Strong EDS peaks of Ag are observed in the as-prepared Ag microsheets, and the other EDS peaks are only attributed to the Si signal from the substrate to hold the Ag microsheet samples (Figure S2 in the Supporting Information), confirming the high purity of metallic Ag sheets. The XRD pattern of the as-prepared Ag microsheets (Figure 1d) shows a sharp and strong diffraction peak together with three weak diffraction peaks, which are indexed to the {111}, {200}, {220}, and {311} planes of the face-centered cubic crystalline structure, respectively. The lattice parameter calculated from the XRD patterns is 4.089 Å, which is also consistent with the JCPDS card no. 04-0783 (α = 4.0862 Å). No other diffraction peaks are observed

DOI: 10.1021/acsami.5b03571
ACS Appl. Mater. Interfaces 2015, 7, 13685−13692

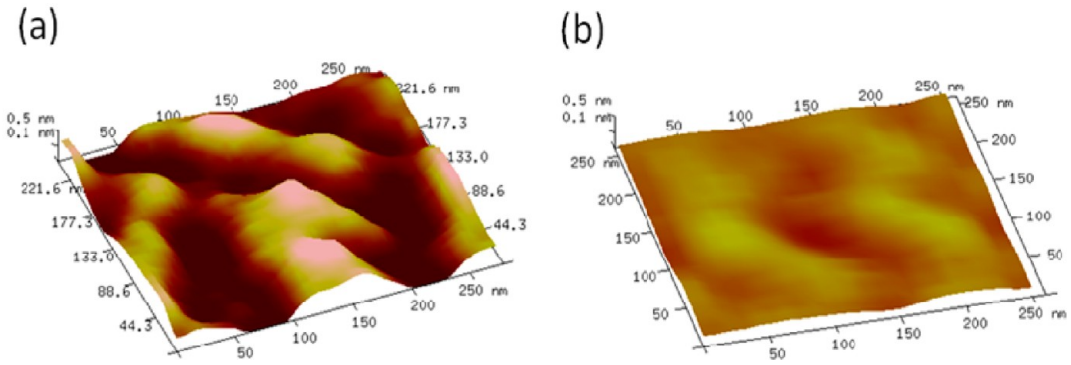

Figure 2. AFM images of (a) commercial and (b) as-prepared silver sheets.

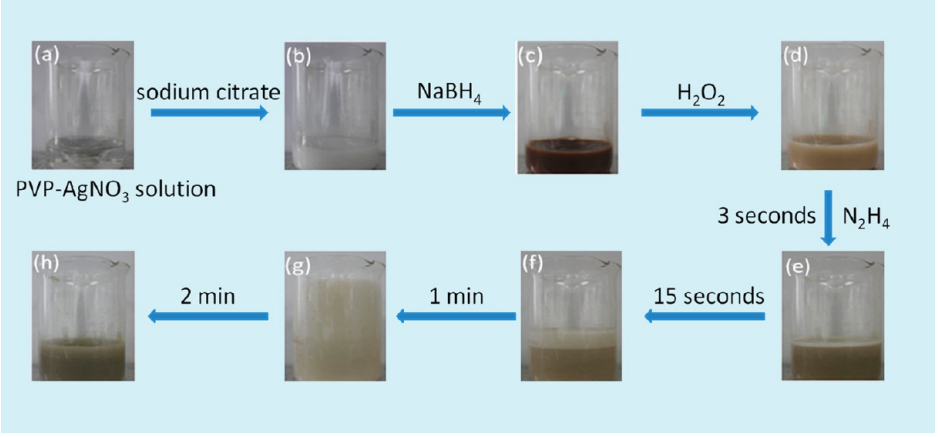

Figure 3. Photographs of the reaction solution during the synthesis process of silver sheets (a) in PVP–$AgNO_3$ solution, (b) after the addition of sodium citrate, (c) after the addition of $NaBH_4$ solution, (d) after the addition of H_2O_2 solution, (e) 3 s after the addition of N_2H_4, (f) 15 s after the addition of N_2H_4, (g) 1 min after the addition of N_2H_4, and (h) 2 min after the addition of N_2H_4.

in the XRD pattern, indicating that the as-prepared samples are of high purity and single-phase. It should be noted that the intensity ratio of the {200} and {111} diffraction peaks is about 0.39, which is lower than the conventional value of 0.45 (JCPDS card no. 04-0783) but much higher than that of the previously reported silver sheets with thickness lower than 28 nm and edge length of about 15 μm[28] or with a thickness of 40 nm and an edge length of about 3–8 μm.[29] It also confirms that the as-prepared silver microsheets exhibit {111} preferential orientation, although they are not as thin as the reported silver sheets.[27−30,32] When functioning as flaky fillers for ECAs, a suitable thickness might be beneficial for preventing the sheets from winding in the mixing or application processes of ECAs to maintain the large face-to-face contact area of conductive silver sheets.

A typical SEM image of traditional commercial silver flakes for ECAs is shown in Figure S3 in the Supporting Information as a comparison. The morphology of as-prepared silver microsheets is obviously different from the traditional commercial silver flakes. The commercial silver flakes prepared by ball-milling are irregular, and the particle size distribution is in a wide range from about 1 to 20 μm. The thickness of ball-milled silver flakes is more than 300 nm, which is larger than that of those obtained in this study. Furthermore, the AFM results (Figure 2) obviously confirm that the surface of ball-milled silver flakes is not as smooth as that of the one-step prepared silver microsheets. The as-prepared silver microsheets might have better conductive performance than the traditional commercial silver flakes when they are used as fillers for ECAs due to their smoother and straighter surface, relatively thin thickness, suitable size, and uniform hexagonal shape.[17] Compared with the traditional ball-milling process, our method has only one step needed to get the microsized silver flakes, avoiding the extra cost of mechanical ball-milling and the impurity pollution involved in the preparation process (Figure S4 in the Supporting Information). The whole procedure is conducted in an aqueous solution at room temperature and under ambient conditions. Finally, the micrometer-sized silver sheets maintain the uniform size and morphology. Thus, this approach has great potential to be applied in the industrial production of Ag microsheets.

3.2. Function of Reagents and Growth Mechanism of Silver Microsheets. During the fabrication process of silver microsheets, the color of the reaction solution changes after each agent addition, as shown in Figure 3. When sodium citrate is added into the colorless $AgNO_3$–PVP solution (Figure 3a), the mixture becomes milk white (Figure 3b) due to the chelation reaction between Ag+ ions and citrate ions in the solution. As the sodium borohydride solution is then added, the color immediately changes to brown (Figure 3c) due to the sodium borohydride reduction of Ag+ ions. The color changes to yellow-gray (Figure 3d), and a few bubbles are observed as the H_2O_2 drops, which might be the result of the oxidization reaction by H_2O_2 to release O_2 gas. After the N_2H_4 addition, lots of gas bubbles appear, and the foam even reaches to the top of beaker (Figure 3e–g) in a few minutes as the N_2H_4 and

DOI: 10.1021/acsami.5b03571
ACS Appl. Mater. Interfaces 2015, 7, 13685−13692

H_2O_2 are decomposed in the reduction of Ag^+ ions. Finally, the color of the solution becomes gray, and precipitates are observed (Figure 3h).

SEM, EDS, XRD, FT-IR, and UV−vis techniques are used to further investigate the products after the addition of each agent in the fabrication of Ag microsheets. Spherical nanoparticles (Figure 4a) are obtained after the sodium citrate is added into the $AgNO_3$−PVP solution. XRD results (Figure S5a in the Supporting Information) suggest that the production is silver citrate (JCPDS card no.01−0030). After the addition of $NaBH_4$ into the solution, the surfaces of the silver citrate spherical nanoparticles become rough (Figure 4b) as the result of a small amount of Ag^+ reduction (Figure S5b in the Supporting Information). Because the amount of the $NaBH_4$ reduction agent is much less than the amount of Ag^+ ions, the main diffraction peaks in Figure S5b (Supporting Information) are still attributed to the silver citrate. The brown color of the solution after the $NaBH_4$ addition might be due to the formation of some Ag nanoparticles on the surfaces of silver citrate spherical nanoparticles. When observed 0.5 h after the addition of H_2O_2, the morphology of the particles is similar to that of the samples collected after the addition of $NaBH_4$, but the size seems smaller, as shown in Figure 4c. This might be the result of the H_2O_2 oxidative reaction, which would form bubbles. The XRD results (Figure S5c in the Supporting Information) also show the near disappearance of diffraction peaks for metallic Ag. Element contents from the EDS (Figure S6a−c in the Supporting Information) and the FT-IR (Figure S7a−c in the Supporting Information) results also indicate that there are obvious carbon and oxygen elements in the products after successive additions of sodium citrate, $NaBH_4$, and H_2O_2 into the $AgNO_3$−PVP solution. Comparing these results to those of the samples collected after the addition of sodium citrate or H_2O_2, there is a peak at about 400 nm in the UV−vis curve that is assigned to spherical Ag nanoparticles for samples collected after addition of $NaBH_4$ (Figure S8a−c in the Supporting Information),[33] confirming the formation of Ag nanoparticles after the addition of $NaBH_4$ and the oxidization of these Ag nanoparticles by H_2O_2.

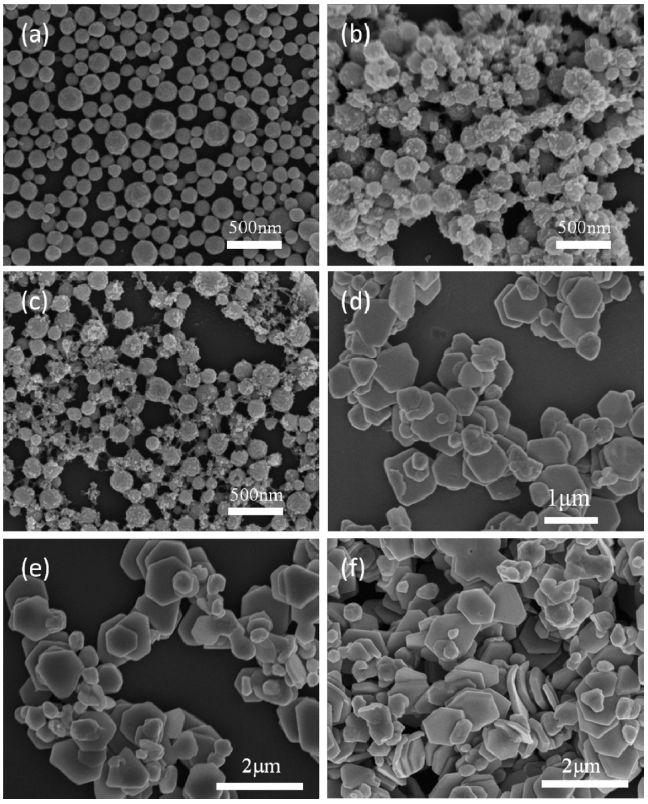

Figure 4. SEM images of samples collected in the synthesis process of silver microsheets (a) after the addition of sodium citrate; (b) after the addition of $NaBH_4$, (c) 0.5 h after the addition of H_2O_2; and (d−f) 3, 10, and 30 min after the addition of N_2H_4.

Precipitates of hexagonal microsheets with small irregular particles (Figure 4d) are collected after the foam's disappearance when N_2H_4 is added (Figure 3h, about 3 min). There are only diffraction peaks of metallic Ag in the XRD pattern of these precipitates (Figure S5d in the Supporting Information). The EDS results (Figure S6d in the Supporting Information) also confirm that the precipitates are metallic Ag. The results indicate that the Ag^+ ions in the chelate could be totally reduced by N_2H_4 to form metallic Ag hexagonal microsheets and small irregular particles in a few minutes at room temperature. As the duration increases from 3 to 30 min, the Ag hexagonal microsheets become more predominant and uniform (Figure 4e,f), and then the nearly hexagonal Ag microsheets are obtained after the addition of N_2H_4 at 2 h (Figure 1a). In addition, the XRD patterns become somewhat sharp (Figure S5e,f in the Supporting Information), indicating the disappearance of small nanoparticles. However, there are no obvious differences in the EDS atomic content results (Figure S6e−f in the Supporting Information), FT-IR curves (Figure S7e,f in the Supporting Information), and UV−vis spectra (Figure S8e,f in the Supporting Information) for the Ag products collected after the addition of N_2H_4 for 3, 10, and 30 min because there is only a little morphology change for the Ag precipitates.

The functions of reagents in the fabrication of silver flakes are also investigated. First, we increase the concentration of $AgNO_3$ in the fabrication. As shown in Figure 5a, there are irregular Ag particles with Ag hexagonal microsheets in the products when the concentration of $AgNO_3$ is increased to 30 mmol/L.

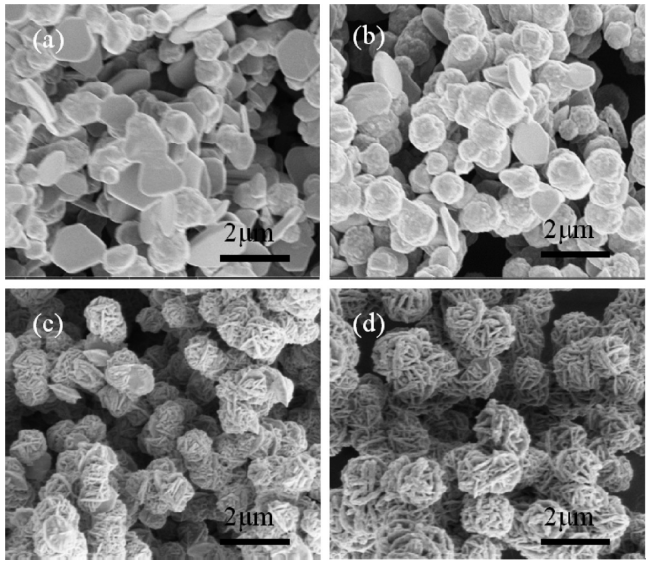

Figure 5. SEM images of the samples prepared with an $AgNO_3$ concentration of (a) 30, (b) 100, (c) 150, and (d) 300 mmol/L.

DOI: 10.1021/acsami.5b03571
ACS Appl. Mater. Interfaces 2015, 7, 13685−13692

Almost no Ag hexagonal microsheets (but spherical particles of about 800 nm) are obtained as the concentration of $AgNO_3$ is increased to 100 mmol/L (Figure 5b). For the higher $AgNO_3$ concentration of 150 or 300 mmol/L, the products are Ag spherical particles of more than 1 μm with very rough surfaces (Figure 5c,d). The orientational growth of the Ag crystal could not be realized for the fast reduction reaction at a high concentration of $AgNO_3$; thus, Ag hexagonal microsheets are not obtained.

As shown in Figure 6a,b and in Figure S9a,b in the Supporting Information, Ag hexagonal microsheets are obtained even when there is no addition of PVP (or of more PVP) in the preparation process. The circumstances of sodium citrate addition (Figure 6c,d and Figure S9c,d in the Supporting Information) are similar to those of PVP, but there are also many smaller irregular particles or triangular sheets in the productions, especially for the samples without the addition of PVP. The sheets prepared without the addition of sodium citrate are bigger compared with those prepared without the addition of PVP; some of them are even larger than 2 μm. These results suggest that the mixture of Ag microsheets and irregular particles could be formed with the addition of PVP or sodium citrate. PVP and citrate are usually used as capping and stabilizing agents in the preparation of silver nanoplates.[25,34] Citrate might easily absorb on the {111} facet, and PVP might preferentially absorb on the {100} facet, respectively.[18,20,29,31,35,36] Thus, these additives could suppress the growth rate of the {111}/{100} planes and stabilize the particles, promoting the formation of hexagonal silver microsheets with a certain thickness.

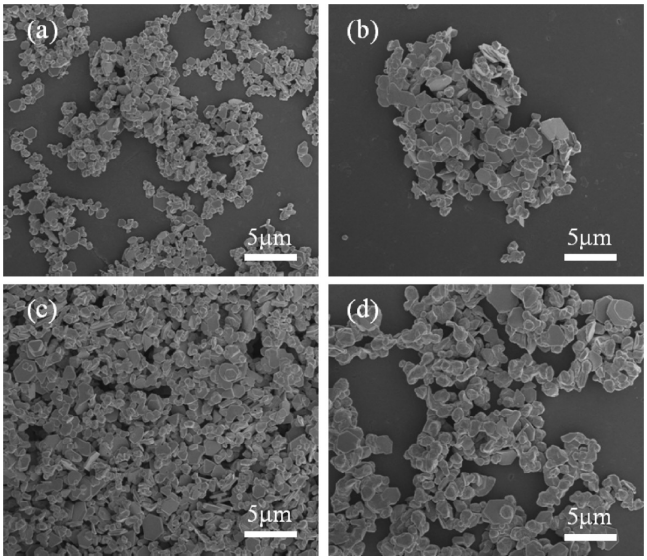

Figure 6. SEM images of the samples prepared (a) without the addition of PVP, (b) with the addition of 5 mmol PVP, (c) without the addition of sodium citrate, and (d) with the addition of 2 mmol sodium citrate.

A few uniform hexagonal Ag microsheets accompanied by irregular Ag particles (Figure 7a and Figure S10a in the Supporting Information) are produced if there is no $NaBH_4$ addition. However, there are Ag particles smaller than 30 nm (Figure 7b and Figure S10b in the Supporting Information) in the resulted samples rather than hexagonal microsheets with addition of more $NaBH_4$ such as 5 mmol in the preparation process. $NaBH_4$ can reduce Ag^+ ions to metallic Ag nanoparticles quickly and eliminate the function of PVP or citrate absorption on the {111}/{100} planes of Ag due to its strong reducing ability. A little bit of $NaBH_4$ might reduce Ag^+ ions to obtain a small amount of silver nanoparticles as seeds for later microsheets growth. But more $NaBH_4$ might consume lots of Ag^+ ions to form too many small nanoparticles in the early stage and inhibit the later growth of microsheets for its strong reduction ability. Only spherical Ag nanoparticles with size smaller than 50 nm (Figure 7c and Figure S10c in the Supporting Information) are obtained and no sheets are generated in the absence of H_2O_2. In contrast, large Ag microsheets (Figure 7d and Figure S10d in the Supporting Information) are produced even if the addition amount of H_2O_2 is doubled (200 mmol). H_2O_2 acts as an oxidative agent to etch irregular and small silver particles then for selective growth of reduced silver atoms, which is like the fabrication of silver nanoplates smaller than 1 μm.[33,37,38] Figure 7e,f and Figure S10e,f in the Supporting Information illustrate that the products are almost silver citrate fibers if no N_2H_4 addition but Ag microsheets and some small particles are obtained for adding more N_2H_4 of 200 mmol. N_2H_4 is used as a major reduction here to completely reduce Ag+ ions with the selectively etching by H_2O_2 to form Ag hexagonal microsheets.

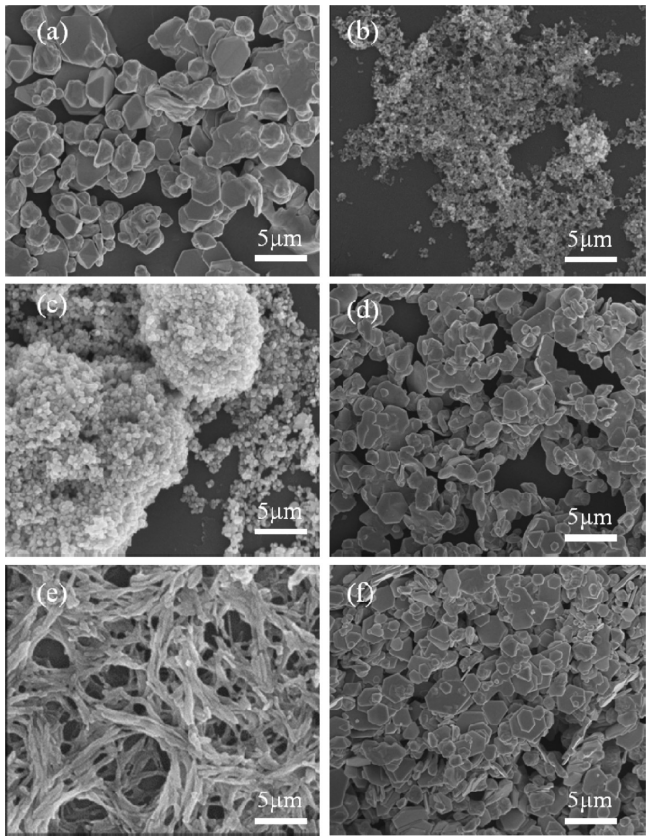

Figure 7. SEM images of the samples prepared (a) without the addition of $NaBH_4$, (b) with the addition of 5 mmol $NaBH_4$, (c) without the addition of H_2O_2, (d) with the addition of 200 mmol H_2O_2, (e) without the addition of N_2H_4, and (f) with the addition of 200 mmol N_2H_4.

According to the above results, a possible mechanism as schematically shown in Figure 8 is proposed to account for the formation of uniform hexagonal Ag microsheets. A small amount of silver nanoparticles are first rapidly reduced from the

DOI: 10.1021/acsami.5b03571
ACS Appl. Mater. Interfaces 2015, 7, 13685−13692

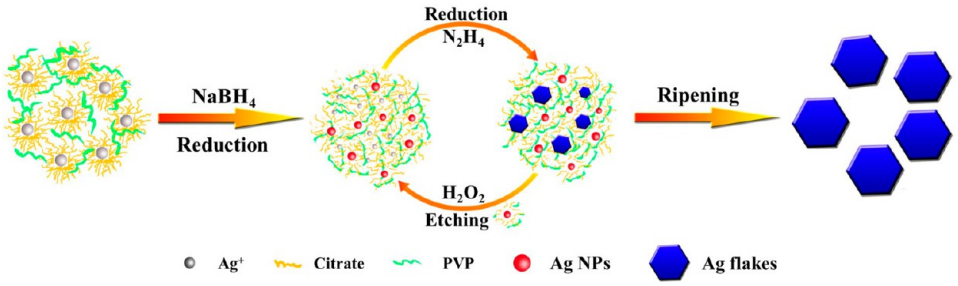

Figure 8. A schematic process for the formation of uniform hexagonal Ag microsheets.

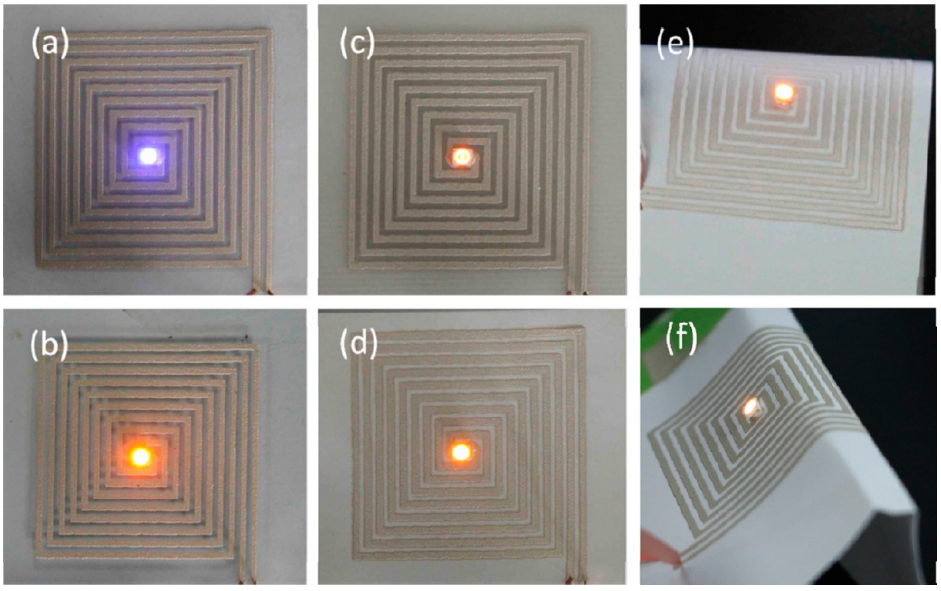

Figure 9. Photos of printed ECA tracks with attached LEDs on different substrates: (a) PET, (b) glass, (c) epoxy, (d) paper, and (e,f) bended papers.

silver citrate by the strong reducing agent of $NaBH_4$ and then stabilized by PVP and citrate. A large amount of Ag^+ ions is still in the silver citrate as a silver resource. The citrate and PVP would absorb on the {111}/{100} facets of metallic silver seeds. The silver atoms freshly reduced by N_2H_4 preferentially grow along the lateral plane, with the synergistic effect of H_2O_2 selectively etching small and irregular Ag particles to form silver hexagonal microsheets. Furthermore, uniform silver hexagonal microsheets are finally obtained in the Ostwald ripening process.

3.3. Printed Electrically Conductive Tracks and Conductivity. As shown in Figure 9, it is easily to print and cure the silver hexagonal microsheet filled epoxy adhesives as conductive fine tracks on different substrates such as PET (Figure 9a), epoxy (Figure 9b), glass (Figure 9c), and paper (Figure 9d). The ECAs can be also used in the flexible substrates such as bended papers, as shown in Figure 9e,f.

To further evaluate the bulk resistivity of the silver−epoxy resin conductive adhesive, we also manually printed liquid silver−epoxy resin conductive adhesives flatly onto a glass substrate, using a small scraper to form a stripe of 6 mm × 75 mm. They were cured at 150 °C for 2 h and cooled to room temperature in an oven. The bulk resistivity of the adhesives is calculated by the following equation:

$$\rho = R\frac{w \times t}{l}$$

where ρ (Ω cm) is the bulk resistivity, R (Ω) is the resistance, w (mm), t (mm), and l (mm) are the width, thickness, and length of the silver−epoxy resin conductive adhesive stripes, respectively. The as-prepared silver hexagonal microsheet filled adhesives demonstrate a bulk resistivity of $8.1 \times 10^{-5} \pm 3\%$ Ω cm, which is considerably lower than that of traditional ball-milled silver-flake-filled adhesives ($1.2 \times 10^{-4} \pm 3\%$ Ω cm) with the same silver content of 80 wt %. The conductivity of as-prepared silver hexagonal microsheet filled adhesives is also better than that of the commercial ECAs or previously reported ball-milled silver-flake-filled ECAs (80 wt % Ag), which usually show resistivity in the range of about 10^{-3} to 10^{-4} Ω cm.[1,39−41] As shown in Figure 10, the as-prepared silver hexagonal microsheets are more uniformly filled and well contacted to each other in the epoxy adhesives relative to those of commercial silver flakes after curing. In addition, the smooth and straight surfaces could enhance the contact interface areas of as-prepared silver hexagonal microsheets. Thus, the as-prepared silver hexagonal microsheet filled ECAs exhibit higher electrically conductive performance than that of traditional ball-milled silver-flake-filled ECAs.

4. CONCLUSIONS

A facile and one-step wet chemical method is demonstrated for the synthesis of uniform silver hexagonal microsheets. The surfaces of the silver microsheets are smooth and straight, with a size of more than 1 μm and a thickness of approximately 200

DOI: 10.1021/acsami.5b03571
ACS Appl. Mater. Interfaces 2015, 7, 13685−13692

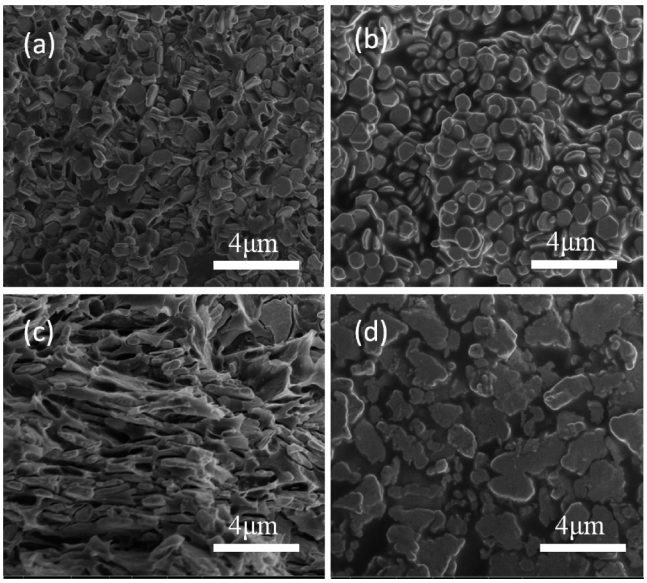

Figure 10. (a,c) Cross-section and (b,d) surface SEM images of the ECAs with fillers of (a,b) as-prepared silver hexagonal microsheets and (c,d) commercial silver flakes.

nm. Polyvinylpyrrolidone and citrate are used as facet-selective capping and stabilizing reagents. $NaBH_4$ is used as a strong reducing reagent to generate nanosized Ag seeds. H_2O_2 acts as selective etching reagent to remove irregular and small Ag particles. The Ag atoms freshly reduced from silver citrate by N_2H_4 then could preferentially grow alone on the {111} facet of Ag seeds to form Ag hexagonal microsheets. The Ag-microsheet-filled ECAs can be easily printed and cured on various substrates such as epoxy, PET, glass, paper, and flexible substrates. The silver hexagonal microsheet filled ECAs exhibit considerably lower bulk resistivity (approximately 8.1×10^{-5} Ω cm) than that of commercial ball-milled silver-flake-filled ECAs (approximately 1.2×10^{-4} Ω cm).

■ ASSOCIATED CONTENT

Supporting Information

SAED and EDS results of as-prepared Ag microsheets, an SEM image of the traditional commercial silver flakes, FT-IR curves of the traditional commercial ball-milled silver flakes and as-prepared Ag microsheets, XRD, EDS, FT-IR, and UV−vis results of samples collected during the synthesis process of silver microsheets, XRD patterns of the resulted samples without and with additional amounts of reagents. The Supporting Information is available free of charge on the ACS Publications website at DOI: 10.1021/acsami.5b03571.

■ AUTHOR INFORMATION

Corresponding Authors

*X.-Z.F. Tel: +86-755-86392151. Fax: +86-755-86392299. E-mail: xz.fu@siat.ac.cn

*S.Y. E-mail: sh.yu@siat.ac.cn

*R.S. E-mail: rong.sun@siat.ac.cn.

Notes

The authors declare no competing financial interest.

■ ACKNOWLEDGMENTS

This work was financially supported by the National Natural Science Foundation of China (no. 21203236), the Guangdong and Shenzhen Innovative Research Team Program (nos. 2011D052 and KYPT20121228160843692), the Shenzhen Electronic Packaging Materials Engineering Laboratory (no. 2012-372), and the Shenzhen High Density Electronic Packaging and Device Assembly Key Laboratory (no. ZDSYS20140509174237196).

■ REFERENCES

(1) Yang, C.; Wong, C. P.; Yuen, M. M. F. Printed Electrically Conductive Composites: Conductive Filler Designs and Surface Engineering. *J. Mater. Chem. C* **2013**, *1*, 4052−4069.

(2) Kim, C.; Nogi, M.; Suganuma, K.; Yamato, Y. Inkjet-Printed Lines With Well-Defined Morphologies and Low Electrical Resistance on Repellent Pore-Structured Polyimide Films. *ACS Appl. Mater. Interfaces* **2012**, *4*, 2168−2173.

(3) Wang, B. Y.; Yoo, T. H.; Song, Y. W.; Lim, D. S.; Oh, Y. J. Cu Ion Ink For a Flexible Substrate and Highly Conductive Patterning by Intensive Pulsed Light Sintering. *ACS Appl. Mater. Interfaces* **2013**, *5*, 4113−4119.

(4) Ahn, B. Y.; Duoss, E. B.; Motala, M. J.; Guo, X. Y.; Park, S. I.; Xiong, Y. J.; Yoon, J.; Nuzzo, R. G.; Rogers, J. A.; Lewis, J. A. Omnidirectional Printing of Flexible, Stretchable, and Spanning Silver Microelectrodes. *Science* **2009**, *323*, 1590−1593.

(5) Li, Z.; Zhang, R.; Moon, K.-S.; Liu, Y.; Hansen, K.; Le, T.; Wong, C. P. Highly Conductive, Flexible, Polyurethane-Based Adhesives for Flexible and Printed Electronics. *Adv. Funct. Mater.* **2013**, *23*, 1459−1465.

(6) Zhang, Y.; Zhu, P. L.; Li, G.; Zhao, T.; Fu, X. Z.; Sun, R.; Zhou, F.; Wong, C. P. Facile Preparation of Monodisperse, Impurity-Free, and Antioxidation Copper Nanoparticles on a Large Scale for Application in Conductive Ink. *ACS Appl. Mater. Interfaces* **2014**, *6*, 560−567.

(7) Zhang, R.; Lin, W.; Moon, K. S.; Wong, C. P. Fast Preparation of Printable Highly Conductive Polymer Nanocomposites by Thermal Decomposition of Silver Carboxylate and Sintering of Silver Nanoparticles. *ACS Appl. Mater. Interfaces* **2010**, *2*, 2637−2645.

(8) Wu, H.; Chiang, S. W.; Lin, W.; Yang, C.; Li, Z.; Liu, J.; Cui, X.; Kang, F.; Wong, C. P. Towards Practical Application of Paper-Based Printed Circuits: Capillarity Effectively Enhances Conductivity of the Thermoplastic Electrically Conductive Adhesives. *Sci. Rep.* **2014**, *4*, 6275−6278.

(9) Li, Z.; Le, T.; Wu, Z.; Yao, Y.; Li, L.; Tentzeris, M.; Moon, K. S.; Wong, C. P. Rational Design of a Printable, Highly Conductive Silicone-Based Electrically Conductive Adhesive for Stretchable Radio-Frequency Antennas. *Adv. Funct. Mater.* **2015**, *25*, 464−470.

(10) Reinhold, I.; Hendriks, C. E.; Eckardt, R.; Kranenburg, J. M.; Perelaer, J.; Baumann, R. R.; Schubert, U. S. Argon Plasma Sintering of Inkjet Printed Silver Tracks on Polymer Substrates. *J. Mater. Chem.* **2009**, *19*, 3384−3388.

(11) Tekin, E.; Smith, P. J.; Schubert, U. S. Inkjet Printing as a Deposition and Patterning Tool for Polymers and Inorganic Particles. *Soft Matter* **2008**, *4*, 703−713.

(12) Li, Y.; Moon, K. S.; Wong, C. P. Electronics Without Lead. *Science* **2005**, *308*, 1419−1420.

(13) Li, Y.; Wong, C. P. Recent Advances of Conductive Adhesives as a Lead-Free Alternative in Electronic Packaging: Materials, Processing, Reliability and Applications. *Mater. Sci. Eng., R* **2006**, *51*, 1−35.

(14) Pu, N. W.; Peng, Y. Y.; Wang, P. C.; Chen, C. Y.; Shi, J. N.; Liu, Y. M.; Ger, M. D.; Chang, C. L. Application of Nitrogen-Doped Graphene Nanosheets in Electrically Conductive Adhesives. *Carbon* **2014**, *67*, 449−456.

(15) Zhang, R.; Moon, K. S.; Lin, W.; Wong, C. P. Preparation of Highly Conductive Polymer Nanocomposites by Low Temperature Sintering of Silver Nanoparticles. *J. Mater. Chem.* **2010**, *20*, 2018−2023.

(16) Wang, J.; Chen, Z.; Hu, Y.; Jiang, X.; Chen, D.; Zhang, W. Flaky Silver Powders Prepared with Nanofilm Transition Method:

DOI: 10.1021/acsami.5b03571
ACS Appl. Mater. Interfaces 2015, 7, 13685−13692

Application for Printable Electronics. *J. Mater. Chem. C* **2013**, *1*, 230−233.
(17) Le Beulze, A.; Duguet, E.; Mornet, S.; Majimel, J.; Treguer-Delapierre, M.; Ravaine, S.; Florea, I.; Ersen, O. New Insights into the Side-Face Structure, Growth Aspects, and Reactivity of Ag_n Nanoprisms. *Langmuir* **2014**, *30*, 1424−1434.
(18) Sun, Y. G.; Xia, Y. N. Shape-Controlled Synthesis of Gold and Silver Nanoparticles. *Science* **2002**, *298*, 2176−2179.
(19) Song, J. L.; Chu, Y.; Liu, Y.; Li, L. L.; Sun, W. D. Room-Temperature Controllable Fabrication of Silver Nanoplates Reduced by Aniline. *Chem. Commun.* **2008**, 1223−1225.
(20) Aherne, D.; Ledwith, D. M.; Gara, M.; Kelly, J. M. Optical Properties and Growth Aspects of Silver Nanoprisms Produced by a Highly Reproducible and Rapid Synthesis at Room Temperature. *Adv. Funct. Mater.* **2008**, *18*, 2005−2016.
(21) Tao, A. R.; Habas, S.; Yang, P. D. Shape Control of Colloidal Metal Nanocrystals. *Small* **2008**, *4*, 310−325.
(22) Pastoriza-Santos, I.; Liz-Marzan, L. M. Colloidal Silver Nanoplates. State of the Art and Future Challenges. *J. Mater. Chem.* **2008**, *18*, 1724−1737.
(23) Liu, X.; Li, L.; Yang, Y.; Yin, Y.; Gao, C. One-Step Growth of Triangular Silver Nanoplates with Predictable Sizes on a Large Scale. *Nanoscale* **2014**, *6*, 4513−4516.
(24) Yang, Y.; Zhong, X. L.; Zhang, Q.; Blackstad, L. G.; Fu, Z. W.; Li, Z. Y.; Qin, D. The Role of Etching in the Formation of Ag Nanoplates with Straight, Curved and Wavy Edges and Comparison of Their SERS Properties. *Small* **2014**, *10*, 1430−1437.
(25) Zhang, Q.; Li, N.; Goebl, J.; Lu, Z.; Yin, Y. A Systematic Study of the Synthesis of Silver Nanoplates: Is Citrate a "Magic" Reagent? *J. Am. Chem. Soc.* **2011**, *133*, 18931−18939.
(26) Kim, B. H.; Oh, J. H.; Han, S. H.; Yun, Y. J.; Lee, J. S. Combinatorial Polymer Library Approach for the Synthesis of Silver Nanoplates. *Chem. Mater.* **2012**, *24*, 4424−4433.
(27) Park, S. H.; Son, J. G.; Lee, T. G.; Park, H. M.; Song, J. Y. One-Step Large-Scale Synthesis of Micrometer-Sized Silver Nanosheets by a Template-Free Electrochemical Method. *Nanoscale Res. Lett.* **2013**, *8*, 248.
(28) Chen, H.; Simon, F.; Eychmuller, A. Large-Scale Synthesis of Micrometer-Sized Silver Nanosheets. *J. Phys. Chem. C* **2010**, *114*, 4495−4501.
(29) Deng, Z.; Mansuipur, M.; Muscat, A. J. New Method to Single-Crystal Micrometer-Sized Ultra-Thin Silver Nanosheets: Synthesis and Characterization. *J. Phys. Chem. C* **2009**, *113*, 867−873.
(30) Yang, J. H.; Lu, L. H.; Wang, H. S.; Shi, W. D.; Zhang, H. J. Glycyl Glycine Templating Synthesis of Single-Crystal Silver Nanoplates. *Cryst. Growth Des.* **2006**, *6*, 2155−2158.
(31) Murshid, N.; Kitaev, V. Role of Poly(vinylpyrrolidone) (PVP) and other Sterically Protecting Polymers in Selective Stabilization of {111} and {100} Facets in Pentagonally Twinned Silver Nanoparticles. *Chem. Commun.* **2014**, *50*, 1247−1249.
(32) Chang, C. W.; Lin, F. C.; Chiu, C. Y.; Su, C. Y.; Huang, J. S.; Perng, T. P.; Yen, T. J. HNO_3-Assisted Polyol Synthesis of Ultralarge Single-Crystalline Ag Microplates and Their Far Propagation Length of Surface Plasmon Polariton. *ACS Appl. Mater. Interfaces* **2014**, *6*, 11791−11798.
(33) Tsuji, M.; Gomi, S.; Maeda, Y.; Matsunaga, M.; Hikino, S.; Uto, K.; Tsuji, T.; Kawazumi, H. Rapid Transformation from Spherical Nanoparticles, Nanorods, Cubes, or Bipyramids to Triangular Prisms of Silver with PVP, Citrate, and H_2O_2. *Langmuir* **2012**, *28*, 8845−8861.
(34) Zhang, Q.; Yang, Y.; Li, J.; Iurilli, R.; Xie, S. F.; Qin, D. Citrate-Free Synthesis of Silver Nanoplates and the Mechanistic Study. *ACS Appl. Mater. Interfaces* **2013**, *5*, 6333−6345.
(35) Wang, Y. X.; Fang, J. Y. Selective Epitaxial Growth of Silver Nanoplates. *Angew. Chem., Int. Ed.* **2011**, *50*, 992−993.
(36) Zeng, J.; Xia, X. H.; Rycenga, M.; Henneghan, P.; Li, Q. G.; Xia, Y. N. Successive Deposition of Silver on Silver Nanoplates: Lateral Versus Vertical Growth. *Angew. Chem., Int. Ed.* **2011**, *50*, 244−249.
(37) Parnklang, T.; Lertvachirapaiboon, C.; Pienpinijtham, P.; Wongravee, K.; Thammacharoen, C.; Ekgasit, S. H_2O_2-Triggered Shape Transformation of Silver Nanospheres to Nanoprisms with Controllable Longitudinal LSPR Wavelengths. *RSC Adv.* **2013**, *3*, 12886−12894.
(38) Li, N.; Zhang, Q.; Quinlivan, S.; Goebl, J.; Gan, Y.; Yin, Y. H_2O_2-Aided Seed-Mediated Synthesis of Silver Nanoplates with Improved Yield and Efficiency. *ChemPhysChem* **2012**, *13*, 2526−2530.
(39) Yang, C.; Lin, W.; Li, Z.; Zhang, R.; Wen, H.; Gao, B.; Chen, G.; Gao, P.; Yuen, M. M. F.; Wong, C. P. Water-Based Isotropically Conductive Adhesives: Towards Green and Low-Cost Flexible Electronics. *Adv. Funct. Mater.* **2011**, *21*, 4582−4588.
(40) Ji, Y. H.; Liu, Y.; Huang, G. W.; Shen, X. J.; Xiao, H. M.; Fu, S. Y. Ternary Ag/Epoxy Adhesive with Excellent Overall Performance. *ACS Appl. Mater. Interfaces* **2015**, *7*, 8041−8052.
(41) Mahajan, A.; Hyun, W. J.; Walker, S. B.; Lewis, J. A.; Francis, L. F.; Frisbie, C. D. High-Resolution High-Aspect Ratio Conductive Wires Embedded in Plastic Substrates. *ACS Appl. Mater. Interfaces* **2015**, *7*, 1841−1847.

DOI: 10.1021/acsami.5b03571
ACS Appl. Mater. Interfaces 2015, 7, 13685−13692